OPEN ACCESS
IOP Publishing
Semiconductor Science and Technology
Semicond. Sci. Technol. **34** (2019) 035028 (9pp)
https://doi.org/10.1088/1361-6641/ab0591

Transition to the quantum hall regime in InAs nanowire cross-junctions

Johannes Gooth[1,2,7,8], **Mattias Borg**[1,9], **Heinz Schmid**[1], **Nicolas Bologna**[1,3], **Marta D Rossell**[1,3], **Stephan Wirths**[1], **Kirsten Moselund**[1], **Kornelius Nielsch**[2,4,5,6] **and Heike Riel**[1,7]

[1] IBM Research-Zurich, Säumerstrasse 4, 8803 Rüschlikon, Switzerland
[2] Institute of Nanostructure and Solid-State Physics, Universität Hamburg, Jungiusstraße 11, D-20355 Hamburg, Germany
[3] Electron Microscopy Center, EMPA, Swiss Federal Laboratories for Materials Science and Technology, Überlandstrasse 129, 8600 Dübendorf, Switzerland
[4] Institute for Metallic Materials, Leibniz Institute for Solid State and Materials Research Dresden, Helmholtzstraße 20, D-01069 Dresden, Germany
[5] Technische Universität Dresden, Institute of Materials Science, D-01062 Dresden, Germany
[6] Technische Universität Dresden, Institute of Applied Physics, D-01062 Dresden, Germany

E-mail: johannes.gooth@outlook.com and hei@zurich.ibm.com

Received 13 November 2018, revised 9 January 2019
Accepted for publication 8 February 2019
Published 25 February 2019

Abstract

We present a low-temperature electrical transport study on four-terminal ballistic InAs nanowire cross-junctions in magnetic fields aligned perpendicular to the cross-plane. Two-terminal longitudinal conductance measurements between opposing contact terminals reveal typical 1D conductance quantization at zero magnetic field. As the magnetic field is applied, the 1D bands evolve into hybrid magneto-electric sub-levels that eventually transform into Landau levels for the widest nanowire devices investigated (width = 100 nm). Hall measurements in a four-terminal configuration on these devices show plateaus in the transverse Hall resistance at high magnetic fields that scale with $(ve^2/h)^{-1}$. e is the elementary charge, h denotes Planck's constant and v is an integer that coincides with the Landau level index determined from the longitudinal conductance measurements. While the 1D conductance quantization in zero magnetic field is fragile against disorder at the NW surface, the plateaus in the Hall resistance at high fields remain robust as expected for a topologically protected Quantum Hall phase.

Supplementary material for this article is available online

Keywords: magneto-transport, nanowire, conductance quantization, InAs, TASE

(Some figures may appear in colour only in the online journal)

Introduction

Semiconductor nanowire (NW) cross-junctions have recently been considered as one of the means to implement interconnected NW network circuitry [1, 2]. In such a scheme, each NW branch is controlled individually *via* local gate transistor nodes, hence giving rise to reconfigurable logic operations. Another possible application of NW cross-junction is in quantum computing technology, [3–7] where ballistic cross-junctions enable the transfer of quantum information between qubits. In this context, InAs is a material

[7] Authors to whom any correspondence should be addressed.
[8] Now at Max Planck Institute for Chemical Physics of Solids, D-01187 Dresden, Germany.
[9] Now at Department of Electrical and Information Technology and NanoLund, Lund University, Box 118, Lund, Sweden.

of particular interest, because it exhibits a low electronic effective mass, a high electron mobility, and strong spin-orbit coupling. Owing to these intriguing properties, individual InAs nanowires have been widely studied in conventional field-effect transistor devices [8–14]. Moreover, quantum transport phenomena were investigated in ballistic one-dimensional NW channels [15–23] and in quantum dots, [24–27] fabricated by introducing defects, axial heterostructures or using top-gates to induce local confinement. In addition, magneto-transport experiments have been performed, [28–33] which are considered an important observable for characterizing the charge transport characteristics in NWs.

Recently, such magnetic field-dependent transport experiments have revealed the crossover from a one-dimensional transport in zero magnetic field towards the selective population of spatially separated edge channels at high magnetic fields [21]. The hallmark of ballistic 1D quantum transport is a step-wise increase of the electrical conductance in units of the conductance quantum $G_0 = 2e^2/h$ as a function of gate voltage when the temperature is so low that thermal excitations across the one-dimensional sub-band gaps at the Fermi level are not possible [18, 34, 35]. Subjecting a 1D quantum wire to an out-of-plane magnetic field B leads to the emergence of Landau quantization and Zeemann-splitting, which causes the degeneration of the Landau levels. When the magnetic length $l_m = (h/2\pi eB)$ becomes larger than the width of the quantum wire, spatially separated counter-propagating edge states are formed, where scattering in a single channel is forbidden and scattering between edge states is exponentially suppressed [21]. Here, e denotes the elementary charge and h is Planck's constant. In principle, these counter-propagating edge states can be observed as quantized Plateaus in the Hall resistance of $R_{xy} = (\nu e^2/h)^{-1}$ that only depend on natural constants and the integer filling factor $\nu = 1, 2, 3, \ldots$ of the system. However, the short NW channel lengths used in the experiment described in [21] did not allow for the attachment of lateral Hall probes. In this regard, III–V semiconductor NW cross-junction devices are particularly interesting because their four-terminal geometry naturally facilitates lateral Hall measurement probes [2, 4, 36–38] and progress in material growth has enabled the observation of ballistic 1D quantum transport in crossed NW devices [35, 39].

Methods

Nanowire device fabrication

For our experiment, we have grown InAs NW cross-junction by template-assisted selective epitaxy (TASE) on SOI within pre-patterned SiO_2 nanotube templates that determine the length, cross-section, position and axial direction of the NW devices. Metal-organic chemical vapor deposition is used to epitaxially grow InAs on Si within the templates. The template design is chosen such that each individual branch is pointing along an $\langle 110 \rangle$ axis of the InAs crystal. Trimethylindium and tertiarybutylarsine are used as precursors in H_2 carrier gas at a total pressure of 60 Torr for the InAs growth at 550 °C. Further details on the growth can be found elsewhere [35, 39–41]. Using electron-beam lithography and lift-off technique, electrical contacts were defined at each NW terminal of the cross-junction. The protective SiO_2 template has been selectively removed in the contact area, using a combination of reactive ion etching and buffered oxide wet etch. Prior to thermal evaporation of the Ni/Au (50 nm/30 nm) contacts, the contact area was immersed in an ammonium sulfide solution for passivation. Importantly, the SiO_2-growth-template protects the InAs NW structures from oxidation and other environmental influences. However, to investigate the effect of scattering at the NW surface, on some of the devices the protective SiO_2 template was removed on the entire device.

To ensure a homogeneous electric field distribution in our devices when tuning the Fermi level, we prepared solid electrolyte gates [13]. Therefore, following the recipe of Liang *et al* [42], a mixture of Polyethyleneoxide(PEO)/$LiClO_4$ (8:1 in weight ratio) dissolved in methanol was spun on the chips at 1500 rpm, followed by a baking process at 90 °C. A sketch of the device is shown in figure 1(a).

Electrical transport experiments

The transport experiments were performed in a temperature variable cryostat (Physical Property Measurement System from Quantum Design) with a base temperature of 2 K in helium atmosphere and equipped with a 9 T magnet. Two electrical contact configurations have been used in our experiments: first, two-terminal transport measurements across two opposed terminals of the NW cross junctions. We refer to measurements in this kind of contact configuration as 'longitudinal' and mark the corresponding transport parameters with the sub-index xx. Bias spectroscopy at zero magnetic field was performed, measuring the current I_{xx} through the devices in response to an applied DC bias voltage V_{xx}. Moreover, the longitudinal magnetoresistance ($R_{xx}(B) = V_{xx}(B)/I_{xx}$) has been measured in this contact configuration. Second, four-terminal transport measurements are performed. In this configuration, a current bias I_{xx} is applied between two opposed terminals of the NW cross and the voltage response V_{yy} on the two opposed terminals transverse to the current-injection terminals is measured. We refer to measurements in this kind of contact configuration as 'transverse' and mark the corresponding transport parameters with the sub-index xy. In this contact configuration the Hall-resistance $R_{xy}(B) = V_{xy}(B)/I_{xx}$ is measured. For the current-bias measurements, a current of 100 nA with standard low frequency ($f = 6$ Hz) lock-in technique is applied. The magnetic field is always applied perpendicular to the x and y-direction ($B = B_z$). Because the liquid ion gate freezes at low temperatures ($T < 250$ K), each measurement is performed at a fixed gate voltage in an individual cool down, taking approximately 90 min each. To avoid hysteresis effects during the temperature cycles, the gate voltage was increased stepwise from −2 to 1 V between the cycles. To solely obtain the

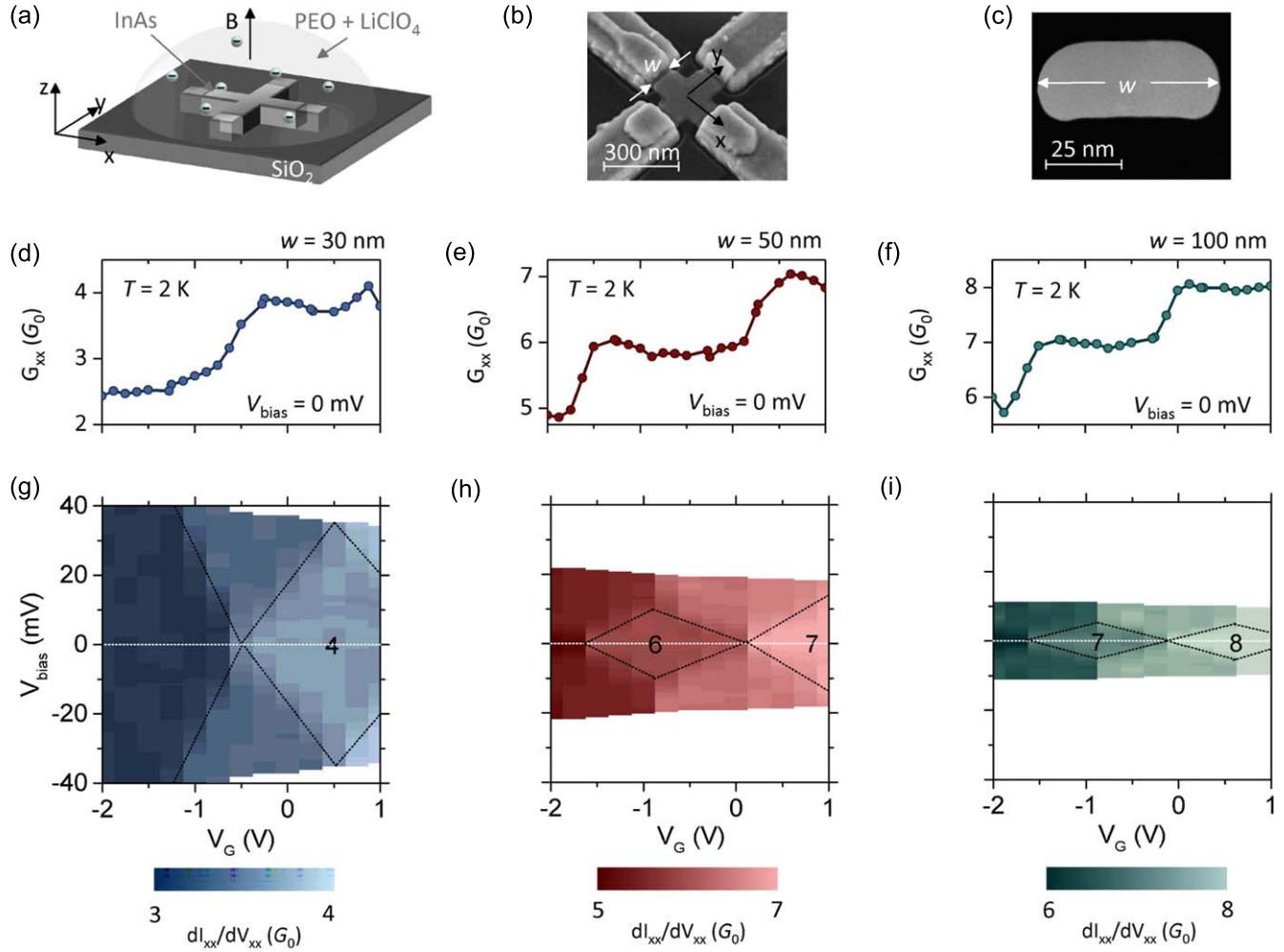

Figure 1. One-dimensional quantized conductance at zero magnetic field. (a) Scheme of the electrical transport device. All four terminals are contacted. An electrolyte gate (PEO + $LiClO_4$) is used to tune the Fermi level of the device. Optionally, a magnetic field B can be applied. (b) Scanning electron beam micrograph of a cross-junction. The InAs channel width w is the same for all terminals. (c) Zero-bias ($V_{bias} = 0$ mV) line cuts of the differential longitudinal conductance $G_{xx} = dI/dV_{bias}$ of a 30 nm-wide, (d) a 50 nm-wide and (e) a 100 nm-wide NW channel. (f) G_{xx}-(V_{gate}, V_{bias}) colour plots of a 30 nm-wide, (g) a 50 nm-wide and (h) a 100 nm-wide NW channel. The numbers denote the index of the individual sub-band.

longitudinal resistance of the InAs cross-junctions, contact resistances of (6.7 ± 0.4) kΩ were subtracted on all low temperature data shown [35, 39]. NW cross-junctions (figure 1(b)) with widths (w = 30, 50 and 100 nm) and a height (h = 25 nm) in the range of the Fermi wavelength λ of InAs (typically $\lambda_{InAs} \approx 35$ nm) [27] are investigated. Hall measurements on our devices at 300 K (supplemental material (SM) is available online at stacks.iop.org/SST/34/035028/mmedia) reveal an electron concentration of about 5×10^{17}cm^{-3} and a mobility between 3700 and 6000 cm^2 V^{-1} s^{-1}, decreasing with shrinking width, which we attribute to increased surface scattering. We note that all obtained results are independent of contact terminal iteration (see SM for details).

Scanning transmission electron microscopy analysis

For structural and compositional analysis of the NW devices, Scanning Transmission Electron Microscopy (STEM) is performed. Cross-sectional lamellas are prepared by means of an FEI Helios Nanolab 450 S focused ion beam instrument operated at accelerating voltages of 30 and 5 kV. STEM imaging and STEM-energy dispersive x-ray spectroscopy (EDX) analysis are performed using a double spherical aberration-corrected microscope (JEOL JEM-ARM200F), operated at 200 kV, and equipped with a silicon drift detector (JEOL Dry SD100GV) with 100 mm^2 detection area for EDX analysis.

Results and discussion

One-dimensional quantized conductance at zero magnetic field

In a first transport experiment, we verify that the InAs nanowire cross-junctions are ballistic 1D quantum wire systems at zero magnetic field. Therefore, low temperature (T = 2 K) bias spectroscopy is performed with no magnetic field applied (B = 0 T). Consistent with our previous studies, [35, 39] the NW cross-junctions exhibit plateaus at integer

multiples n of $2e^2/h$ shown in the zero-bias ($V_{\mathrm{bias}} = 0$ mV) line cuts of the differential longitudinal conductance $G_{xx} = \mathrm{d}I/\mathrm{d}V_{\mathrm{bias}}$ (figures 1(c)–(e))-the hallmark of ballistic 1D quantum transport [17, 18, 22]. As expected from the simple model of an infinite 1D quantum well, the energy level spacing $\Delta E_{i,j}$, given by the tips of the diamond-like structures in the 2D G_{xx}-(V_{gate}, V_{bias}) colour plots of figures 1(f)–(h), resembles the 1D sub-band splitting of the previously investigated single InAs NWs [35] and InAs NW cross-junctions [39]. Also, consistently, the smaller the NW channel width, the larger the size quantization and thus the gapping of the 1D sub-bands ($w = 30$ nm: $\Delta E_{3,4} = 35$ meV; $w = 50$ nm: $\Delta E_{5,6} = 12$ meV; $w = 50$ nm: $\Delta E_{6,7} = 8$ meV). We note that despite the similar carrier concentrations for zero gate voltage at 300 K, the sub-band population at 2 K depends on the NW channel width. This is, because the thermal activation energy becomes smaller than the size of the sub-band spacing and thus the point in V_{G} where transport through the 1D states commences is linked to the strength of the size quantization at low temperatures. In comparison to previously investigated back-gated devices, no full pinch-off is reached in any device, because the 20 nm-thick template oxide weakens the effect of the liquid ion gate.

One-dimensional sub-band depopulation in low magnetic field

Next, we investigate the evolution of the 1D features within a magnetic field. When applying a magnetic field B perpendicular to the plane of the cross-junction, we observe a stepwise increase of $R_{xx}(B)$ in multiples of G_0^{-1} at low B (figures 2(a)–(c)). This is a signature of Landau quantization and corresponds to the magnetic depopulation of the 1D sub-bands with increasing field [43, 44]. Compared to previous studies on InSb [5, 17] and InAs [22] NWs at mK temperatures, where indications for Zeeman-split sub-bands of lifted spin-degeneracy are observed, which is reflected by half-integer $(G_0/2)^{-1}$-features between the resistance plateaus, such features are not obvious from our raw data. This is probably due to the finite current bias as well as the elevated base temperature used in our experiment. However, as shown later, signatures of Zeeman splitting can be obtained by further data processing. At magnetic fields above 5 T, the plateau-like 1D levels in the magnetoresistance of the widest cross-junction ($w = 100$ nm) evolve into peaks. Such transition in the Landau level spectrum is a first indication for a transformation of the electronic structure in these NW structures [45].

Magnetic field-dependence of the sub-bands

To investigate this transition in more detail, we calculate the derivative of the inverse longitudinal resistance with respect to the gate voltage $g = \mathrm{d}(1/R_{xx})/\mathrm{d}V_{\mathrm{G}}$, which relates to the magnetoelectric band structure of the NW devices. The results for the 30 nm-wide device is shown in figure 2(d)), for the 50 nm-wide device in figure 2(e) and for the 100 nm-wide device in figure 2(f)) [5, 17, 22]. Because in 1D, the transition between the longitudinal resistance plateaus is linked with the onset of transport in an additional sub-band, the maxima of g can be associated with the sub-band energies. For all investigated NW samples, the sub-bands are indexed with n, starting from the zero-field plateau values. n scales non-linear with inverse magnetic field, consistent with a continuous depopulation of the 1D states. Zeeman splitting of the sub-bands is reflected by branching of the individual maximum-traces at high magnetic field as indicated by arrows (spin up and spin down) [20–22]. In addition, plotting the filling factor $\nu = 2n$ into fan diagrams (figures 2(g)–(i)), provides fingerprints of a transition from size quantization at zero B-field to Landau quantization in high fields as indicated by the grey dotted lines: [44, 46] Being non-linear at high $1/B$-values (low magnetic fields), the index-plots exhibit a linear relation between ν and $1/B$ at low $1/B$-values (high fields), tracing the theoretical description of Shubnikov-de Haas oscillations. The emergence of this linear relation is expected in the limit, where the Landau level splitting $\Delta E_B = \dfrac{heB}{2\pi m^*}$ greatly exceeds the 1D sub band spacing $\Delta E_{i,j}$ [44, 46]. Employing the effective mass of bulk InAs $m^* = 0.023m_0$, we find the centres of the 1D–2D transition ($\Delta E_B = \Delta E_{i,j}$) at around $B = 7$ T, 4 T and 1.2 T for the 30 nm-wide, the 50 nm-wide and the 100 nm-wide NW channels, respectively. These results agree reasonable well with a size-dependent, smooth crossover from 1D conductance quantization to hybrid magnetoelectric sub-bands in our InAs NW cross-junction data, eventually transforming into edge states for the 100 nm-wide devices in high B [47].

Quantum hall regime at high magnetic field

Having established the transformation from one-dimensional bulk states in low B to edge-channels in high B using longitudinal transport parameters, we now turn to investigate the Hall resistance R_{xy} of the NW cross-junctions. For the 30 nm-wide and the 50 nm-wide NW channels, the Hall response under applied magnetic field is strongly suppressed and no significant voltage signal could be measured. This may be explained by the fact that for the magnetic field range applied, the electron-trajectories cannot enter a side probe directly, since their cyclotron radii are larger than the widths of the side arms. In the case of the 100 nm-wide device, however, we measure a Hall response above 0.5 T and observe well-defined integer quantum Hall plateaus $R_{xy} = (ve^2/h)^{-1}$ for $B > 5$ T (figure 3(a)), which position in B matches the position of the above the minima of the longitudinal resistance data. In the extreme quantum limit, the R_{xx} is expected to vanish in the quantum Hall state. R_{xx} in the InAs NW system, however, remains finite, which could be explained by the finite temperature and limited magnetic field range investigated or parallel conduction paths of surface and bulk. For clarity reasons, a smooth 2nd order polynomial background is subtracted from R_{xx} to obtain ΔR_{xx} (figure 3(b)) as is usually done to distinguish the Shubnikov-de Haas oscillations on the surface of topological insulators from the bulk. The 1D sub-bands, which carry the current at zero field seem to be smoothly transformed into edge channels when exposed to an out-of-plane magnetic field. Our observation is concurrent with

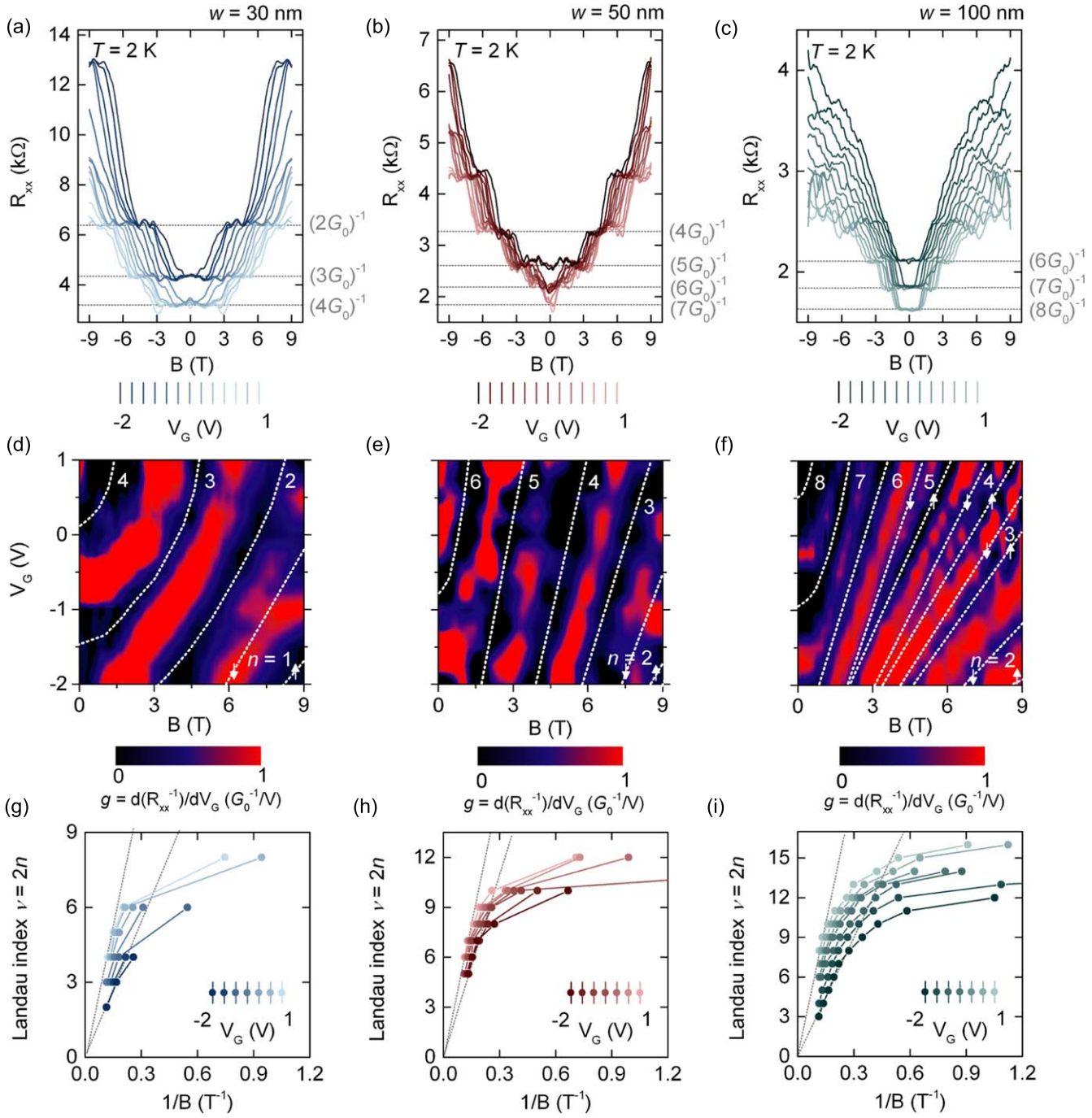

Figure 2. Magnetoelectric sub-band structure. (a) Longitudinal electrical resistance $R_{xx}(B) = V_{xx}(B)/I_{xx}$ at 2 K for various gate voltages V_G of a 30 nm-wide, (b) a 50 nm-wide and (c) a 100 nm-wide NW channel. At low magnetic fields, the magnetoresistance scales in steps of the inverse multiples of the conductance quantum $(nG_0)^{-1} = (n2e^2/h)^{-1}$. (d)–(f) Longitudinal differential inverse resistance $g = \mathrm{d}(1/R_{xx})/\mathrm{d}V_G$ as function of gate voltage V_G and perpendicular magnetic field B for each channel width. The onset of the sub-bands is represented by the minima and indexed with integers n. Spin-splitting at higher field is marked by arrows (spin up and down). The white dotted lines are guides to the eyes. (g)–(h) Landau-index $\nu = 2n$ fan diagrams for various gate voltages. The grey lines represent the 2D limit at high magnetic fields.

the recent interpretation of Landau level formation in InAs NW QPCs [21]. Further, as the B field is decreased, R_{xy} exhibits the tendency of a last plateau near $B = 0\,\mathrm{T}$ (see SM for details). This is a feature of 1D confinement, [46, 48] which originates from the fact that at small magnetic fields the Landau level splitting does not become arbitrary small, but evolves into the discrete 1D sub-band splitting.

Robustness of the quantum hall state

Finally, we investigate the robustness of the QH state in the cross-junction. The edge channels are predicted to be topologically protected and therefore expected to be immune to disorder. In a 100 nm-wide NW sample, both ballistic 1D transport at zero field and the QH state at high magnetic fields

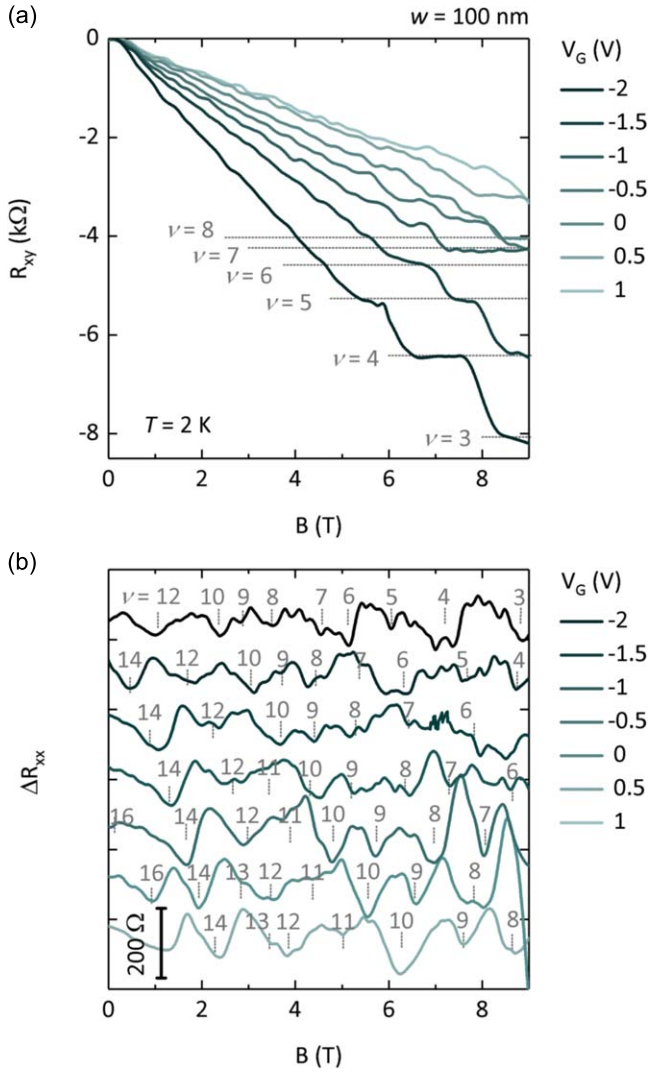

Figure 3. Hall effect in InAs nanowire cross junctions. (a) Hall resistance $R_{xy} = V_{xy}(B)/I_{xx}$ of a 100 nm-wide NW cross-junction at 2 K for various gate voltages V_G as a function of magnetic field B. For $B > 5$ T, plateaus scaling with $(\nu e^2/h)^{-1}$ occur. (b) Residual resistance ΔR_{xx} for the same device at 2 K for various gate voltages V_G as a function of magnetic field B. To obtain ΔR_{xx}, a smooth polynomial background is subtracted from R_{xx}. The minima denote the Landau level ν, indexed by grey numbers.

are observable. By introducing random surface charges, we disturb the ballistic condition along the nanowire axis at zero magnetic field; thus, the quantized resistance plateaus of $(n2e^2/h)^{-1}$ should be suppressed, in contrast to the edge channels of the QH state which are not localized, due to the topological protection, as long as the disorder does not create inelastic scattering events. To carry out this test, we compare the devices protected by the SiO_2 template with devices, on which scattering is purposely induced at the surface of the NW cross-junction by removing the protective SiO_2 template in diluted hydrofluoric acid and subsequently storing the samples for 6 d in air. It is well-known that the electronic transport properties of III–V NW surfaces are modified when subjected to ambient conditions, [49] with the dominant mechanism being carrier scattering at the surface. This is due to the creation of dangling bonds, trap states, surface dipoles and surface oxides that not only induce a morphological disorder, but also impact the electronic band structure of the surface [49].

To address the effect of template-removal in more detail, the surface of both types of devices was investigated by energy dispersive x-ray (EDX) spectroscopy analysis in STEM mode. The line-cut data, taken as indicated in figures 4(a) and (b), reveals that compared to the protected NW (figure 4(c)), the template-removing procedure leads to the formation of a 6 nm-thick non-stochiometric phase at the NW surface (figure 4(d)) that modifies the electronic properties. In magneto-transport experiments (figures (e), (f)), we confirm that the quantized conductance steps at low magnetic fields are clearly suppressed in cross-junction with the disordered surface. Around zero magnetic field, a resistance peak is observed, which is a signature of weak localization [42]-a quantum mechanical interference effect that is caused by closed-loop elastic scattering paths. As the magnetic field is increased, the magnetoresistance exhibits a maximum at around $B_c = 1.3$ T, marking the chambers field, which is explained by surface wall scattering: [50] this arises when bulk scattering is small and low magnetic fields force the electrons against the sidewalls of the NW channel. Disorder at the surface will then cause scattering and the magnetoresistance increases as the magnetic field is enhanced. However, when B is increased further, such that magnetic confinement in the NW channel becomes smaller than the spatial confinement, surface scattering is reduced and the magnetoresistance decreases again. Consistent with this interpretation, the determined $B_c = 5$ T agrees well with the centre of the transition from the 1D conductance quantization to the QH regime in the template-protected samples. At higher magnetic fields, the minima on the smoothly varying background resemble the minima, indexed by ν in the longitudinal magnetoresistance of the protected InAs NW cross-junction (figure 4(e)). This indicates that at high B the sub-band structure of the as-grown NW is recovered, despite the disorder at the surface. Consistently we observed that, while ballistic 1D transport in zero magnetic is fragile against disorder at the NW surface, the QH plateaus at high magnetic fields remain robust. Consequently, R_{xy}, measured on the disordered cross-junction shows distinct plateaus, centred on the minima of the R_{xx}-B data. The height of the plateaus agrees well with the Hall data obtained for the protected NW structure $R_{xy} = (\nu e^2/h)^{-1}$ for $B > B_c = 5$ T and is therefore consistent with the Landau-level-interpretation of the maximum in R_{xx} above. This concludes that the observed QH state is robust against disorder, which is strong enough to supress the transmission of 1D modes at zero magnetic field. A similar test has recently been carried out on Bi_2Se_3 NWs, [51] demonstrating topological protection of helical surface modes. We therefore believe that the robustness of the QH state observed in here, is a strong signature for topologically protected edge channel transport in InAs NW cross-junctions at high magnetic fields. However, we note that at high magnetic fields, the smooth background of the R_{xx}-B has

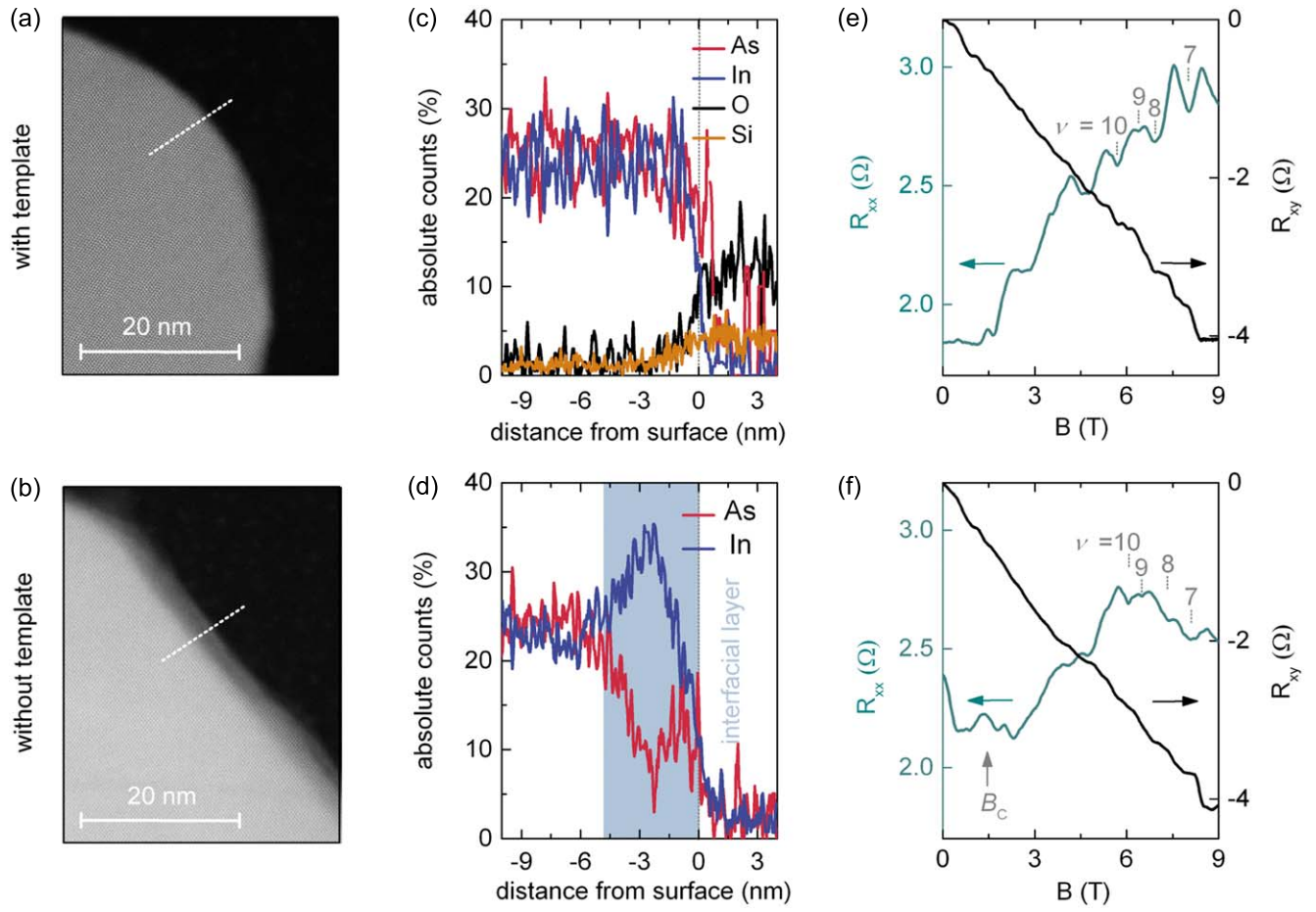

Figure 4. Comparison of template-protected and air-exposed NW devices. (a) Scanning transmission micrograph of an InAs NW channel (light grey area) within the template and (b) after removing the template. (c), (d) STEM-EDX line profiles obtained along the white dotted lines in panels a and b. While the stoichiometry of the protected NW channel is InAs 1:1 at the NW/template interface, the NW with removed template exhibits an indium-rich surface layer of about 6 nm. (e) Magneto-transport data at zero gate voltage and 2 K for a 100 nm-wide NW cross-junction before and (f) after removing the template. The ballistic 1D transport is fragile against the disorder at the channel's surface. A weak-localization peak evolves around $B = 0$ and Chambers peaks of boundary scattering, marked by B_c are observed when the template is removed. At high magnetic fields, the sub-band structure and the Hall plateaus of the disordered device resemble the features observed for the protected NW.

changed, the reason for which is not clear and requires further investigation.

Conclusion

In conclusion, we have implemented ballistic 1D NWs with well-controlled cross-section into a crossbar geometry and provided the first demonstration of a protected QH state in these systems. Magneto-transport experiments reveal that the ballistic 1D quantum system at zero field smoothly evolves into the QH regime in perpendicular magnetic fields. Careful material design, enabled by the TASE process, was critical to study this transition. As expected from theory, [45] the transition from 1D to the QH regime occurs around the same B-field ($B_c = 5$ T), where the magnetic confinement overcomes the spatial size confinement. The template-protected devices enabled an exploration of ballistic 1D transport and test its stability upon inducing disorder at the NW surface. While the ballistic transmission of 1D modes was supressed, the edge channel transport in the QH state remained robust, which we believe provides evidence for topological protection. Therefore, such NW quantum Hall devices can be useful for applications in fault-tolerant quantum computing and non-dissipative electronic devices. However, there are still two main obstacles to overcome: the QH state only exists at low temperatures and high magnetic fields. Following the example of the quantum spin Hall effect in 2D quantum wells, [52, 53] topologically protected edge channel transport without magnetic field might also be obtainable in future 1D NW devices.

Acknowledgments

The authors acknowledge W Hansen for fruitful discussions. We thank M Tschudy for metallization of the devices and technical support. The research leading to these results has received funding from the European Union's Horizon 2020 research and innovation program under grant agreement No

687931 'REMINDER', the European Union Seventh Framework Programs (FP7/2007–2013), No. 619509 'E2SWITCH', the Marie Curie Post-Doctoral Research Fellowship No. 704045 'MODES', and, also the Rudolf Diesel Industry Fellowship funded by the EU Marie Curie Cofund Program (FP7-MC-COFUND, grant agreement No. 291763), and also the Swiss National Science Foundation (SNSF) with project no. 200021_156746.

Associated content

The supporting material includes Hall measurements of all devices at 300 K, the magneto-transport data of the 100 nm-wide device at 2 K and zero gate voltage with iterated terminals as well as a zoom-in to the suppressed Hall resistance around zero magnetic field and Hall traces of all devices investigated at 2 K.

Author contributions

JG and MB conceived the original idea for the study. MB, HS and SW synthesized the InAs nanowires. MB and JG fabricated the NW devices. JG carried out the transport measurements. NB and MR. carried out the STEM-EDX analysis. JG MB. and HS analyzed the data. HR, KM and KN supervised the project. All authors contributed to the interpretation of the data and to the writing of the manuscript.

Funding sources

European Union's Horizon 2020 research and innovation program under grant agreement No 687931 'REMINDER', the European Union Seventh Framework Programs (FP7/2007–2013), No. 619509 'E2SWITCH', the Marie Curie Post-Doctoral Research Fellowship No. 704045 'MODES', and, also the Rudolf Diesel Industry Fellowship funded by the EU Marie Curie Cofund Program (FP7-MC-COFUND, grant agreement No. 291763).

Competing interests

The authors declare no competing interests.

Data availability

All data generated or analyzed during this study are included in this published article (and its Supplementary Material files).

ORCID iDs

Johannes Gooth https://orcid.org/0000-0002-4062-3232
Mattias Borg https://orcid.org/0000-0003-1217-369X

References

[1] Ferry D K 2008 Nanowires in nanoelectronics *Science* **319** 579
[2] Heedt S, Vakulov D, Rieger T, Rosenbach D, Trellenkamp S, Grützmacher D, Lepsa M I and Schäpers T 2016 Electronic properties of complex self-assembled InAs nanowire networks *Adv. Electron. Mater.* **2** 1500460
[3] Gooth J, Borg M, Schmid H, Schaller V, Wirths S, Moselund K, Luisier M, Karg S and Riel H 2017 Ballistic one-dimensional InAs nanowire cross-junction interconnects *Nano Lett.* **17** 2596–602
[4] Plissard S R *et al* 2013 Formation and electronic properties of InSb nanocrosses *Nat. Nanotechnol.* **8** 859–64
[5] Fadaly E M T, Zhang H, Conesa-Boj S, Car D, Gül Ö, Plissard S R, Op het Veld R L M, Kölling S, Kouwenhoven L P and Bakkers E P A M 2017 Observation of conductance quantization in InSb nanowire networks *Nano Lett.* **17** 6511–5
[6] Das A, Ronen Y, Most Y, Oreg Y, Heiblum M and Shtrikman H 2012 Zero-bias peaks and splitting in an Al-InAs nanowire topological superconductor as a signature of majorana fermions *Nat. Phys.* **8** 887–95
[7] Mourik V, Zuo K, Frolov S M, Plissard S R, Bakkers E P a. M and Kouwenhoven L P 2012 Signatures of majorana fermions in hybrid superconductor-semiconductor nanowire devices *Science* **336** 1003–7
[8] del Alamo J A 2011 Nanometre-scale electronics with III–V compound semiconductors *Nature* **479** 317–23
[9] Riel H, Wernersson L-E, Hong M and del Alamo J A 2014 III–V compound semiconductor transistors—from planar to nanowire structures *MRS Bull.* **39** 668–77
[10] Dayeh S A, Aplin D P R, Zhou X, Yu P K L, Yu E T and Wang D 2007 High electron mobility InAs nanowire field-effect transistors *Small* **3** 326–32
[11] Burke A M, Carrad D J, Gluschke J G, Storm K, Fahlvik Svensson S, Linke H, Samuelson L and Micolich A P 2015 InAs nanowire transistors with multiple, independent wrap-gate segments *Nano Lett.* **15** 2836–43
[12] Storm K, Nylund G, Samuelson L and Micolich A P 2012 Realizing lateral wrap-gated nanowire FETs: controlling gate length with chemistry rather than lithography *Nano Lett.* **12** 1–6
[13] Carrad D J, Burke A M, Lyttleton R W, Joyce H J, Tan H H, Jagadish C, Storm K, Linke H, Samuelson L and Micolich A P 2014 Electron-beam patterning of polymer electrolyte films to make multiple nanoscale gates for nanowire transistors *Nano Lett.* **14** 94–100
[14] Lind E, Persson A I, Samuelson L and Wernersson L E 2006 Improved subthreshold slope in an InAs nanowire heterostructure field-effect transistor *Nano Lett.* **6** 1842–6
[15] Tian Y, Sakr M R, Kinder J M, Liang D, MacDonald M J, Qiu R L J, Gao H J and Gao X P A 2012 One-dimensional quantum confinement effect modulated thermoelectric properties in InAs nanowires *Nano Lett.* **12** 6492–7
[16] Gooth J, Schaller V, Wirths S, Schmid H, Borg M, Bologna N, Karg S and Riel H 2017 Ballistic one-dimensional transport in InAs nanowires monolithically integrated on silicon *Appl. Phys. Lett.* **110** 083105
[17] Van Weperen I, Plissard S R, Bakkers E P A M, Frolov S M and Kouwenhoven L P 2013 Quantized conductance in an InSb nanowire *Nano Lett.* **13** 387–91
[18] Kammhuber J *et al* 2016 Conductance quantization at zero magnetic field in InSb nanowires *Nano Lett.* **16** 3482–6
[19] Abay S, Persson D, Nilsson H, Xu H Q, Fogelström M, Shumeiko V and Delsing P 2013 Quantized conductance and its correlation to the supercurrent in a nanowire connected to superconductorS *Nano Lett.* **13** 3614–7
[20] Heedt S, Traverso Ziani N, Crépin F, Prost W, Trellenkamp S, Schubert J, Grützmacher D, Trauzettel B and Schäpers T

2017 Signatures of interaction-induced helical gaps in nanowire quantum point contacts *Nat. Phys.* **13** 563–7
[21] Heedt S, Manolescu A, Nemnes G A, Prost W, Schubert J, Grützmacher D and Schäpers T 2016 Adiabatic edge channel transport in a nanowire quantum point contact register *Nano Lett.* **16** 4569–75
[22] Heedt S, Prost W, Schubert J, Grützmacher D and Schäpers T 2016 Ballistic transport and exchange interaction in InAs nanowire quantum point contacts *Nano Lett.* **16** 3116–23
[23] Zota C B, Lindgren D, Wernersson L-E and Lind E 2015 Quantized conduction and high mobility in selectively grown InxGa1–xAs nanowires *ACS Nano* **9** 9892–7
[24] Björk M T, Fuhrer A, Hansen A E, Larsson M W, Fröberg L E and Samuelson L 2005 Tunable effective g factor in InAs nanowire quantum dots *Phys. Rev.* B **72** 201307
[25] Wallin D, Fuhrer A, Fröberg L E, Samuelson L, Xu H Q, Hofling S and Forchel A 2007 Detection of charge states in nanowire quantum dots using a quantum point contact *Appl. Phys. Lett.* **90** 172112
[26] Fasth C, Fuhrer A, Samuelson L, Golovach V N and Loss D 2007 Direct measurement of the spin-orbit interaction in a two-electron InAs nanowire quantum dot *Phys. Rev. Lett.* **98** 266801–4
[27] Wu P M, Gooth J, Zianni X, Svensson S F, Gluschke J G, Dick K a, Thelander C, Nielsch K and Linke H 2013 Large thermoelectric power factor enhancement observed in InAs nanowires *Nano Lett.* **13** 4080–6
[28] Blömers C, Lepsa M I, Luysberg M, Grtzmacher D, Lüth H and Schäpers T 2011 Electronic phase coherence in InAs nanowires *Nano Lett.* **11** 3550–6
[29] Vigneau F, Prudkovkiy V, Duchemin I, Escoffier W, Caroff P, Niquet Y-M, Leturcq R, Goiran M and Raquet B 2014 Magnetotransport subband spectroscopy in InAs nanowires *Phys. Rev. Lett.* **112** 76801
[30] Dhara S, Solanki H S, Singh V, Narayanan A, Chaudhari P, Gokhale M, Bhattacharya A and Deshmukh M M 2009 Magnetotransport properties of individual InAs nanowires *Phys. Rev.* B **79** 121311
[31] Liang D and Gao X P A 2012 Strong tuning of rashba spin-orbit interaction in single InAs nanowires *Nano Lett.* **12** 3263–7
[32] Roulleau P, Choi T, Riedi S, Heinzel T, Shorubalko I, Ihn T and Ensslin K 2010 Suppression of weak antilocalization in InAs nanowires *Phys. Rev.* B **81** 155449
[33] Liang D, Sakr M R and Gao X P A 2009 One-dimensional weak localization of electrons in a single InAs nanowire *Nano Lett.* **9** 1709–12
[34] Sch T and Gr P 2016 Ballistic transport and exchange interaction in InAs nanowire quantum point contacts *Nano Lett.* **16** 3116–163123
[35] Gooth J, Schaller V, Wirths S, Schmid H, Borg M, Bologna N, Karg S and Riel H 2017 Ballistic one-dimensional transport in InAs nanowires monolithically integrated on silicon *Appl. Phys. Lett.* **110** 83105
[36] Blömers C, Grap T, Lepsa M I, Moers J, Trellenkamp S, Grützmacher D, Lüth H and Schäpers T 2012 Hall effect measurements on InAs nanowires *Appl. Phys. Lett.* **101** 152106–10
[37] Storm K, Halvardsson F, Heurlin M, Lindgren D, Gustafsson A, Wu P M, Monemar B and Samuelson L 2012 Spatially resolved hall effect measurement in a single semiconductor nanowire *Nat. Nanotechnol.* **7** 718–22
[38] Hultin O, Otnes G, Borgström M T, Björk M, Samuelson L and Storm K 2016 Comparing hall effect and field effect measurements on the same single nanowire *Nano Lett.* **16** 205–11
[39] Gooth J, Borg M, Schmid H, Schaller V, Wirths S, Moselund K, Luisier M, Karg S and Riel H 2017 Ballistic one-dimensional InAs nanowire cross-junction interconnects *Nano Lett.* **17** 2596–602
[40] Schmid H, Borg M, Moselund K, Gignac L, Breslin C M, Bruley J, Cutaia D and Riel H 2015 Template-assisted selective epitaxy of III–V nanoscale devices for co-planar heterogeneous integration with Si *Appl. Phys. Lett.* **106** 233101
[41] Borg M, Schmid H, Moselund K E, Cutaia D and Riel H 2015 Mechanisms of template-assisted selective epitaxy of InAs nanowires on Si *J. Appl. Phys.* **117** 144303–9
[42] Liang D and Gao X P A 2012 Strong tuning of rashba spin-orbit interaction in single InAs nanowires *Nano Lett.* **12** 3263–7
[43] Van Wees B J, Kouwenhoven L P, Van Houten H, Beenakker C W J, Mooij J E, Foxon C T and Harris J J 1988 Quantized conductance of magnetoelectric subbands in ballistic point contacts *Phys. Rev.* B **38** 3625–7
[44] Tso H C and Vasilopoulos P 1991 Magnetotransport along a quantum wire *Phys. Rev.* B **44** 12952–8
[45] Chu D P and Butcher P N 1993 Intrinsic integer quantum Hall effect in a quantum wire *Phys. Rev.* B **47** 10008–11
[46] Roukes M L, Scherer A, Allen S J, Craighead H G, Ruthen R M, Beebe E D and Harbison J P 1987 Quenching of the hall effect in a one-dimensional wire *Phys. Rev. Lett.* **59** 3011–4
[47] Ando T 1990 Edge states in quantum wires in high magnetic fields *Phys. Rev.* B **42** 5626–34
[48] Beenakker C W J and Van Houten H 1988 Quenching of the hall effect *Phys. Rev. Lett.* **60** 2406–9
[49] Thathachary A V, Agrawal N, Liu L and Datta S 2014 Electron transport in multigate InxGa1-x as nanowire FETs: from diffusive to ballistic regimes at room temperature *Nano Lett.* **14** 626–33
[50] Thornton T J, Roukes M L, Scherer A and Van De Gaag B P 1989 Boundary scattering in quantum wires *Phys. Rev. Lett.* **63** 2128–31
[51] Hong S S, Zhang Y, Cha J J, Qi X L and Cui Y 2014 One-dimensional helical transport in topological insulator nanowire interferometers *Nano Lett.* **14** 2815–21
[52] Bernevig B A, Hughes T L and Zhang S-C 2006 Quantum spin hall effect and topological phase transition in HgTe quantum wells *Science* **314** 1757–61
[53] König M, Wiedmann S, Brüne C, Roth A, Buhmann H, Molenkamp L W, Qi X-L and Zhang S-C 2007 Quantum spin hall insulator state in HgTe quantum wells *Science* **318** 766–70